Physics – Uspekhi **67** (11) 1069 – 1083 (2024)

REVIEWS OF TOPICAL PROBLEMS

PACS numbers: **07.60. – j**, **32.50. + d**, **87.64. – t**

55th ANNIVERSARY OF THE INSTITUTE OF SPECTROSCOPY
OF THE RUSSIAN ACADEMY OF SCIENCES (ISAN)

Optical methods for detection of single biomolecules: visualization, sensorics, sequencing of DNA molecules

P N Melentiev, A S Kalmykov, A S Gritchenko, M P Shemeteva, A M Safonova, M S Markov, V I Balykin, A S Bukatin, N V Vaulin, D A Belov, A A Evstrapov, D A Baklykov, A V Andriyash, A A Barbasheva, A K Kuguk, V V Ryzhkov, I A Rodionov, D S Kudryavtsev, V A Mozhaeva, L V Son, V I Tsetlin, B N Khlebtsov, M S Kobzev, Yu O Kuznetsova, B T Sharipov, A S Yashkin, Ya I Alekseev

DOI: https://doi.org/10.3367/UFNe.2024.07.039720

Contents

1. **Introduction** 1069
2. **Optical and nanophotonic technologies used in optical methods of detection of single molecules** 1070
3. **Detection of individual biomolecules using the example of troponin molecules visualization in human blood** 1074
4. **Detection of virulent virus particles using the example of SARS-CoV-2 coronavirus visualization** 1076
5. **Visualization of toxin–receptor interaction at single-molecule level** 1077
6. **Single-molecule DNA sequencing** 1078
7. **Conclusion** 1081

References 1082

Abstract. A brief overview of the state of the art in optical methods for detecting a single molecule in biomedical applications is presented. It is shown that the registration of fluorescence of single dye molecules covalently bound to antibodies (biomolecules), together with the use of modern nanophotonics methods, can be used to solve various problems in biology and medicine: visualization of biomolecules, toxins, and virus particles; determination of extremely low concentrations of analytes directly in a sample without using methods for increasing the analyte concentration; and optical single-molecule sequencing of DNA molecules. The existing physical limitations of the methods of optical detection and counting of single molecules and their impact on solving existing problems in biology, medicine, and genetics are discussed.

Keywords: nanophotonics, nanoplasmonics, sensorics of ultra-low concentrations of analytes, detection of single molecules, biovisualization, zero-mode waveguides, single-molecule sequencing

P N Melentiev [1, *], **A S Kalmykov** [1], **A S Gritchenko** [1], **M P Shemeteva** [1], **A M Safonova** [1], **M S Markov** [1], **V I Balykin** [1], **A S Bukatin** [2], **N V Vaulin** [2], **D A Belov** [2], **A A Evstrapov** [2], **D A Baklykov** [3], **A V Andriyash** [3], **A A Barbasheva** [4], **A K Kuguk** [4], **V V Ryzhkov** [4], **I A Rodionov** [4], **D S Kudryavtsev** [5], **V A Mozhaeva** [5], **L V Son** [5], **V I Tsetlin** [5], **B N Khlebtsov** [6], **M S Kobzev** [7], **Yu O Kuznetsova** [7], **B T Sharipov** [7], **A S Yashkin** [7], **Ya I Alekseev** [2, 7]

[1] Institute of Spectroscopy, Russian Academy of Sciences, ul. Fizicheskaya 5, 108840 Troitsk, Moscow, Russian Federation
[2] Institute for Analytical Instrumentation, Russian Academy of Sciences, ul. Ivana Chernykh 31-33, lit. A, 198095 St. Petersburg, Russian Federation
[3] Dukhov Research Institute of Automatics, ul. Sushchevskaya 22, 119017 Moscow, Russian Federation
[4] Bauman Moscow State Technical University, ul. 2-ya Baumanskaya 5/1, 105005 Moscow, Russian Federation
[5] Shemyakin–Ovchinnikov Institute of Bioorganic Chemistry, Russian Academy of Sciences, ul. Miklukho-Maklaya 16/10, 117997 Moscow, Russian Federation
[6] Institute of Biochemistry and Physiology of Plants and Microorganisms, Saratov Scientific Center, Russian Academy of Sciences, prosp. Entuziastov 13, 410049 Saratov, Russian Federation
[7] Syntol Ltd., Timiryazevskaya ul. 42, korp. B, office 316, 127434 Moscow, Russian Federation
E-mail: [*] melentiev@isan.troitsk.ru

Received 13 March 2024, revised 16 July 2024
Uspekhi Fizicheskikh Nauk **194** (11) 1130 – 1145 (2024)
Translated by V L Derbov

1. Introduction

The detection and visualization of single atoms and molecules have always been one of the priority tasks in various fields of knowledge, representing enormous scientific and practical significance: the study of quantum electrodynamics effects [1–3], development of single-atom/single-molecule devices [4–7], visualization of biological tissues [8, 9], observation of the kinetics of intracellular chemical reactions [10], studies of the intracellular dynamics of biomolecules [11], measurement of the influence of fluctuations in the local concentration of molecules on cell growth [12], and many others [13–16].

In addition to the monitoring of single molecules, single molecule detection and registration methods have found application in the determination of macroscopic parameters, namely in the measurement of the concentration of substances when the concentration of the desired molecules in a sample (analyte molecules) is extremely low. If the average distance between the analyte molecules

is significantly greater than the wavelength of the light, the macroscopic optical properties of the medium do not depend on the presence of the analyte molecules in the medium, so that conventional optical detection methods (not based on counting individual molecules) are insensitive. Such concentrations are called ultralow, and single molecule counting methods (SMCMs) are used for their direct measurement without using methods for preconcentration of analyte molecules in a sample (enrichment on a functionalized surface of a substrate or micro/nanoparticles, using the polymerase chain reaction [17]) [17–19].

The possibilities of optical registration of single biomolecules using of nanoplasmonics, nanooptics, and integrated photonics have made it possible to implement the most accurate methods of DNA sequencing; the corresponding commercially available devices are called 'single-molecule sequencers.' These devices reveal the nucleotide sequence of a DNA molecule during replication (copying) with the help of the polymerase enzyme at the level of a single DNA molecule by optically detecting the successive events of the incorporation of individual nucleotides and determining their type. Commercial sequencing devices based on optical methods of single-molecule sequencing enable high accuracy and long read length of the nucleotide sequence in a DNA molecule as well as the determination of the entire genome of organisms in the shortest possible time.

This paper presents the results of studies aimed at applying the methods of single molecule counting, nanooptics, and nanoplasmonics to a number of scientifically and practically significant problems: (1) visualization and determination of the concentration of troponin-T molecules in human blood, which are a biomarker in the early stages of human cardiovascular diseases, (2) sensing and determination of the degree of virulence of SARS-CoV-2 coronavirus particles, (3) measurement of receptor–toxin interactions at the single-molecule level, (4) single-molecule optical sequencing of DNA molecules, including the creation of the first sequencer of its kind in Eurasia.

2. Optical and nanophotonic technologies used in optical methods of detection of single molecules

In this paper, we consider methods for detecting and counting single molecules using only optical methods [20] and do not consider other known approaches [21]. It is believed that Moerner was the first to demonstrate optical detection of single molecules, which subsequently stimulated numerous studies in this area [22]. We note the pioneering work of Russian authors in the field of optical registration and spectroscopy of single atoms and molecules [23–26]. Unfortunately, all methods for detecting single molecules are slow. Without a significant increase in the speed of single molecule detection, its use in solving practically important problems turns out to be impossible, e.g., when measuring analyte concentration, a fundamentally important parameter in sensor applications. Thus, for many applications, it is not enough to detect individual analyte molecules only.

Let us consider in more detail the idea of measuring the concentration of an analyte using SMCMs. So, analyte molecules are sequentially detected in a sample one after another, and the number N of molecules in the sample volume V is determined, which allows us to measure the concentration of analyte molecules n as $n = N/V$. The counting of individual molecules is digital: each molecule generates a signal that can be recorded, and the total number of molecules in a known volume can be counted. For the most accurate determination of the concentration of an analyte, it is important to measure the presence or absence of small signals with high reliability (presence/absence of a molecule), rather than measuring the absolute value of a signal proportional to the number of molecules in the sample and determining the desired value of the analyte concentration by calibration. In other words, counting individual molecules is more accurate than the integral assessment of the signal from them. It is believed that the future of all analytical measurements is associated with the use of single molecule counting methods [20].

Single molecule imaging and SMCM sensors are based on counting events corresponding to the detection of single molecules in a volume. In the case of liquid media, analyte molecules are constantly moving due to Brownian motion and thus enter and exit the detection volume, i.e., the physical volume in which a single molecule can be registered using an optical microscope. The value of this volume depends on the type of optical microscopy technique used (epifluorescence, confocal, etc.) and is a function of the optical microscope's field of view, resolution, and effective depth of focus of the objective [27]. For single molecule detection, it is appropriate to speak of the maximum value of the registration volume, upon entering which the molecule can be registered. As will be shown below, when recording the fluorescence of a single molecule in known optical microscopy techniques, such a volume is determined by the resolution of the selected optical scheme. The task of significantly increasing the detection volume is critically important for the creation of sensor platforms with rapid determination of the concentration of analyte molecules, as well as for the possibility of simultaneous monitoring of a large number of single molecules at the same time. This task can be solved using nanolocalized sources of high-intensity radiation or special nanostructures, which in both cases allow an effective increase in the signal-to-noise ratio when registering the fluorescence of a single molecule.

Long-term monitoring of the number of molecules passing through the detection volume can be used to measure the analyte concentration. The counting is associated with molecular shot noise, which is a function of Poisson sampling. In this case, the accuracy of concentration measurements, limited by the signal-to-noise ratio (SNR), is determined by the relationship $\mathrm{SNR} = \sqrt{N}$, as a result of which molecular shot noise significantly affects the determined value of the analyte concentration [28]. Thus, to achieve high detection accuracy, corresponding to an error (defined as the square root of the number of measured molecules) of 1%, at least 10,000 analyte molecules must be measured in the sample. With a typical detection time of one second per molecule (optical detector exposure), the corresponding measurements will take at least three hours.

At ultra-low analyte concentrations, the measurement time is even longer. Thus, at an analyte concentration of about 10^7 molecules cm^{-3} (17 fM), the average distance between molecules is about 45 μm. This distance is orders of magnitude greater than the typical dimensions of the registration volume of a single molecule. To detect 10,000 molecules, in this case, it is necessary to study the presence of analyte molecules in a volume of at least 1 μl. If about 1 s is required to detect one analyte molecule in the

registration volume (~ 1 fl $= 10^{-15}$ l), then about 10^9 s, i.e., decades, is required to analyze a volume of 1 μl (to detect all molecules in the sample volume)!

All known SMCMs solve the problem of low concentration by using a preconcentration step before the detection step. In this way, a dilute solution containing a few molecules can be converted into a smaller volume of much higher concentration. The most common approach in the preconcentration step is to capture the analyte molecules on the surface and then detect them (where the surface concentration is still low, requiring detection of single molecules). The main problem with this approach is the long time required to capture of the molecules. The dynamics of immobilization of analyte molecules on the surface is determined by the Langmuir binding isotherm [29]. For a concentration of 1 fM molecules, the process of their binding to the antibody-functionalized surface will require about a year to reach equilibrium [30]. Commercially available assay kits use the initial part of the binding curve — it is believed that one hour of binding is sufficient to capture enough molecules to measure their concentration in the analyte sample, but the validity of this statement is still disputed [31]. It should also be noted that, there is a loss of analytes with each preconcentration method.

In the fluorescence microscopy scheme, tightly focused laser radiation resonantly excites the fluorescence of the molecule being studied. The fluorescence of the molecule occurs at a shifted frequency, which allows it to be detected against the parasitic background that occurs due to the high power of the laser radiation exciting the molecule. It is believed that the main difficulty in optical registration of a single molecule consists in observing the fluorescence signal against the background of parasitic fluorescence. This problem becomes dominant when working with living objects in biological fluids or buffer solutions with a high level of background luminescence.

The photon flux from a single excited fluorescent molecule is determined by two main factors. The first is the rate of excitation of the molecule by laser radiation, which directly depends on the radiation intensity and reaches a maximum when that intensity is equal to the saturation intensity of the molecule optical transition (the transition between its electronic energy levels). The second is the relaxation rate of the excited state of the molecule, γ, determined by the structure of the molecular electronic energy levels. The maximum photon flux from one molecule can reach values of about $10^5 - 10^6$ photons s^{-1}.

A separate complex technical problem is to detect photons emitted by a single molecule. The measured signal includes three components: (1) fluorescence of the molecule, (2) luminescence of the medium surrounding the molecule, (3) self-noise of the photodetector. The main source of the background signal is the luminescence of various materials (substrates, solvents). Background luminescence has a wide spectrum, which often makes it impossible to detect the fluorescence of molecules [32]. Background luminescence can significantly exceed the fluorescence of the molecule under study if the excitation conditions of the molecule are incorrectly chosen.

A common method for reducing background luminescence is to use strong focusing of laser radiation, as well as confocal detection using microscope objectives with a numerical aperture (NA) of up to 1.49 [33]. Using such approaches, it is possible to achieve a registration volume of approximately $\lambda^3/30$, where λ is the laser wavelength. Indeed, in the case of classical microscopy, the registration volume is limited by the waist of the light beam, the waist width being equal to the diameter of the diffraction-limited spot [27]

$$w_0 = \frac{r_\perp}{2} \approx 0.61 \, \frac{\lambda}{\mathrm{NA}} \, \frac{1}{2}$$

and the focal depth determined by the Rayleigh length

$$\Delta z = 2 z_\mathrm{R} = \frac{2\pi w_0^2 n}{\lambda} \, .$$

For the registration volume V_det, we obtain the expression

$$V_\mathrm{det} = r_\perp^2 \Delta z \approx 0.069 \, \frac{\pi n \lambda^3}{\mathrm{NA}^4} \, .$$

When using confocal microscopy to calculate the registration volume of single-molecule fluorescence, it is necessary to multiply the excitation and detection functions of fluorescence [27]. The transverse resolution in confocal microscopy is expressed as $r_\perp = 0.61\lambda/(\mathrm{NA})$, and the axial resolution, as $r_\parallel = 2n\lambda/(\mathrm{NA}^2)$. When multiplying Gaussian functions, the transverse resolution is equal to

$$r_{\perp,\mathrm{conf}} \approx \frac{0.61}{\sqrt{2}} \, \frac{\lambda}{\mathrm{NA}} \, ,$$

and the longitudinal one is

$$r_{\parallel,\mathrm{conf}} \approx \frac{1}{\sqrt{1 + (0.093\pi)^2}} \, \Delta z \, .$$

Thus, the registration volume in the confocal case is equal to

$$V_\mathrm{det}^\mathrm{conf} = \frac{V_\mathrm{det}}{2\sqrt{1 + (0.093\pi)^2}} \approx \frac{V_\mathrm{det}}{2} \, .$$

If we take the limiting numerical aperture of modern immersion objectives to be equal to $\mathrm{NA} = 1.49$, then the registration volume for confocal detection can be estimated as

$$V_\mathrm{det}^\mathrm{conf} = \frac{1}{2} \, V_\mathrm{det} \cong \frac{1}{2} \, \frac{\lambda^3}{15} = \frac{\lambda^3}{30} \, .$$

Registration of fluorescence occurs in a spectral window of about 100 nm, located in the long-wavelength region of the spectrum relative to the laser line. The fluorescence cross section of dye molecules is several orders of magnitude greater than the parasitic luminescence cross section, so that even such a large registration volume (equal to 0.01 fl), in comparison with the size of a molecule, makes the fluorescence of the molecule significantly greater than the background luminescence.

In ultra-low concentration sensorics, the average distance L between analyte molecules in a solution is much greater than the wavelength of radiation λ. The concentration of the analyte n is directly related to the average distance L between the analyte molecules as $L = 1/\sqrt[3]{n}$. In this case, the probability of detecting a molecule is proportional to

$$\frac{V_\mathrm{det}}{L^3} = \frac{\lambda^3/30}{L^3} = 0.03 \left(\frac{\lambda}{L} \right)^3 ;$$

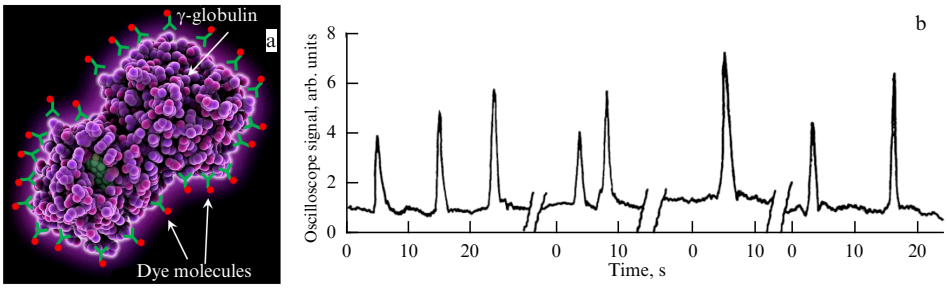

Figure 1. Optical detection of γ-globulin molecule: (a) schematic representation of γ-globulin molecule with $\sim 80-100$ dye molecules attached to it, (b) measured optical signal from oscilloscope; each peak corresponds to detecting a single γ-globulin molecule [46].

here, $V_{\text{det}} = \lambda^3/30$ is the registration volume when using a confocal optical detection scheme. Since we are considering the case $L \gg \lambda$, we obtain a trivial consequence — the probability of detecting molecules in the registration volume turns out to be practically zero. Such a limitation hinders the development of low concentration measurement methods based on counting single molecules, since it leads to extremely long measurement times for reasonable values of analyte volume [20].

The most effective methods for optical detection of single molecules are based on fluorescence. However, most molecules do not fluoresce, so direct optical detection of single molecules by fluorescence becomes impossible. The conventional detection method is based on selective binding of the molecule to fluorescent labels, usually fluorescent dye molecules. Selective labeling can be achieved by selective interactions with ligand binding, e.g., by binding an antibody to an antigen. In this case, the brightness of the nanolocalized radiation sources used — light nanoprobes — is of fundamental importance, since it allows the use of objectives with a small numerical aperture, an increase in the registration area on the sample, and a significant reduction in the detection time of the single-molecule fluorescence.

In the problems of visualization, sensorics, and detection [34, 35], organic dyes [36], quantum dots [37], nanoparticles with up-conversion of light [38], and fluorescent proteins [39] are widely used as nanoprobes of light. A search is underway for alternative methods of creating nanolocalized light sources. Thus, spectrally bright light sources are actively being developed, in which the width of the emission lines is significantly less than 30 nm, the minimum value of the spectral width of emission from quantum emitters at room temperature, determined by phonon broadening [40]. One of the approaches being developed is the use of an active medium placed around a plasmonic nanoparticle in a core–shell configuration in the strong optical coupling mode to generate light with a spectrally narrow line, about 5 nm (when using strong pumping of the active medium [41]), as well as in the weak pumping mode [42]. It is worth noting successes in the creation of light nanoprobes based on silver nanoclusters with a spectral line of less than 5 nm [43], the creation of light sources coupled to nanowaveguides [44], and the possibility of controlling fluorescence using metamaterials [45].

When registering biomolecules that have a relatively large size and, accordingly, a large number of amino acids to attach antibodies, another approach is also used, namely, increasing the photon flux in the registration of a single molecule. This method was first used in 1976 for the optical registration of the γ-globulin molecule [46]. In this paper, the detection of a single biomolecule became possible due to the attachment of about 80–100 dye molecules to it (Fig. 1a). Thus, the appearance of a single molecule in the optical registration area is accompanied by a bright flash of light, registered on an oscilloscope by a signal in the form of a single peak. This, in turn, opens up fundamentally new possibilities in SMCMs, as well as in the visualization of single biomolecules, since it allows a significant, by several orders of magnitude, increase in the registration volume and, consequently, a sharp reduction in the analysis time of practically significant volumes of analyte (Fig. 1b).

In addition to the low fluorescence intensity of a single fluorophore molecule, the total number of photons that can be recorded from a single molecule is limited by the process of its photodegradation [47]. It should be noted that the use of strong optical coupling of dye molecules with plasmonic nanoparticles allows a significant decrease in the rate of photodegradation by reducing the probability of optical transitions to triplet levels responsible for the chemical destruction of the molecule upon interaction with oxygen [48, 49].

The main approach to improving the registration of weak optical signals is to reduce parasitic illumination. In optical microscopy, sharp focusing and confocal microscopy allow the volume of registration and signal collection to be reduced to sizes on the order of the wavelength (Fig. 2a). A further step in increasing the signal-to-noise ratio in optical microscopy of single molecules is proceeding to a subdiffraction registration volume. This can be realized using single metal nanostructures [50, 51] and nanoplasmonics and plasmonic optics methods to enhance local fields [52, 53]. Some of the most suitable nanostructures for detecting single molecule fluorescence are those made in an opaque metal film, so-

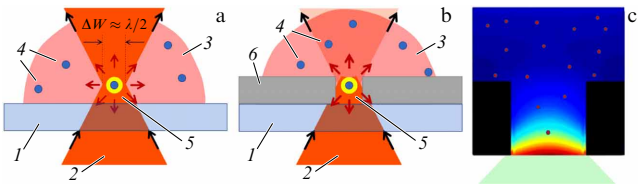

Figure 2. Methods of single molecule detection: (a) single molecule counting in a tightly focused laser beam, (b) molecule detection in zero-mode waveguides. Notation in the diagram: *1* — quartz substrate, *2* — laser radiation, *3* — fluorescent molecules in a buffer solution, *4* — single dye molecules, *5* — excited and emitting dye molecule, *6* — thin aluminum film, (c) field distribution (electric component) inside a zero-mode waveguide.

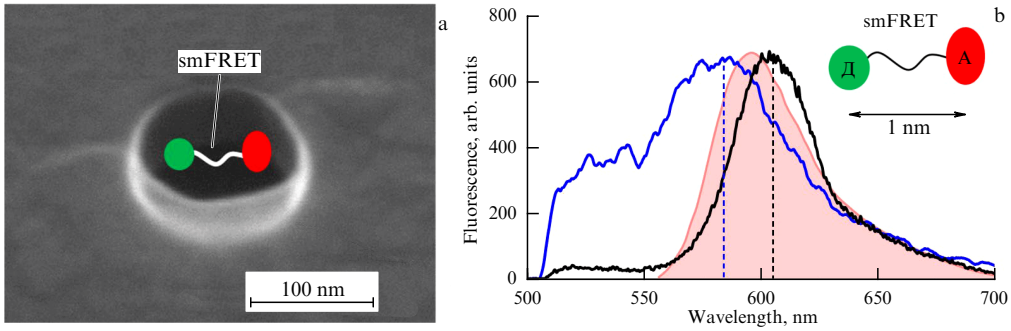

Figure 3. Single-molecule smFRET (FAM-ROX) fluorescence in a single ZMW nanohole: (a) schematic of smFRET molecule arrangement in a ZMW nanohole, imaged by an electron microscope, (b) measured smFRET molecule fluorescence spectra in free space (black curve) and inside the ZMW (blue curve). Fluorescence spectrum of free ROX molecule is shown in pink.

called zero-mode waveguides (ZMWs). ZMW nanostructures are small-diameter nanoholes, about 100 nm in diameter, fabricated in an optically opaque metal film about 100 nm thick (Fig. 2b). The ZMW nanostructure forms an optical waveguide, which, due to its subwavelength dimensions, blocks the propagation of the electromagnetic field, which, when exposed to exciting radiation, allows the energy to be localized in the region of the substrate surface, forming the bottom of the ZMW nanostructure, in a volume much smaller than the wavelength of light (Fig. 2c). This nanowaveguide does not support propagating modes, which explains the use of the name 'zero-mode waveguide' for such a nanostructure [54].

In addition to reducing the recording volume and decreasing the parasitic signal, zero-mode waveguides possess a number of other advantages. The first is that it is possible to conduct studies at the single-molecule level at fairly high analyte concentrations in solution. Indeed, the effective recording and fluorescence collection volume is at the level of 0.1 attoliter (1 attoliter = 10^{-18} l), which allows recording the signal of single molecules at an average concentration of about 10^{15} cm^{-3}. When using conventional optical methods, such as confocal microscopy, the signal is collected from a volume that is more than 2 orders of magnitude greater than the recording volume in the zero-mode waveguide, which does not allow recording single molecules at high analyte concentrations.

The interaction of light with a hole (an aperture made in metal film) with a diameter smaller than the wavelength of light was first considered by Hans Bethe in the 1940s [55]. The problem of interaction of light with a nanohole is also fundamental in modern nanooptics. In the 2000s, with the development of methods for creating nanostructures, such as optical, electron, and ion lithography [56], it was possible to create nanoholes of sufficiently high quality and experimentally demonstrate the detection of fluorescence from single molecules obtained in zero-mode waveguides [57].

Spectral measurement and optical detection of single molecules simultaneously in an array of ZMW nanostructures turned out to be in very high demand for searching the required reactions and compounds and in the development and testing of drugs and various chemical compounds for their toxicity, where it is necessary to make many identical measurements [58].

Currently, this field is rapidly being developed, associated with the creation of biosensors based on ZMW arrays [56]. Reaction cells constructed using zero-mode waveguides allow a significant increase in the sensitivity of fluorescence sensor methods and make it possible to determine low concentrations of substances. On the other hand, ZMW allows studying chemical processes, including biochemical ones, with relatively high concentrations characteristic of living organisms [54]. Thus, ZMW is used to solve a wide range of problems associated with optical detection and spectroscopy; the analysis of chemical and biochemical reactions [59], including multiplex detection [60]; and the analysis of electrochemical processes [61]. Due to the small registration volume, it became possible to measure the dynamics of processes occurring in the membranes of living cells [62].

Placing fluorescent objects inside zero-mode waveguides leads to significant changes in their optical and spectral characteristics. A nanohole in a metal film is a plasmonic resonator; placing quantum emitters in the field of such a resonator allows the rate of radiative processes to increase. The degree of amplification is described by the Purcell factor, which is directly proportional to the resonator quality factor and inversely proportional to its volume [63]. The small volume of the zero-mode waveguide has a significant effect on the emission rate, despite the low quality factor of such resonators. As our recent measurements have shown, the fluorescence spectra of hybrid donor–acceptor molecules (containing fluorophores at a distance of about 1 nm from each other and having mutually overlapping emission and emission spectra, forming the so-called Förster pair of molecules, smFRET) in free space and in ZMW differ significantly. In the measurements, fluorescein (FAM) with a high quantum efficiency (QE), QE = 0.93, was used as a donor; rhodamine X (ROX) with QE = 1 was used as an acceptor. The donor and acceptor molecules are connected by a 1-nm-long linker (Fig. 3a). The estimated Förster radius (R_0) for the FAM-ROX smFRET molecules under consideration in an aqueous buffer solution is $R_0 \approx 6$ nm.

A Nikon inverted microscope was used to measure the fluorescence of smFRET molecules. A buffer solution with FAM-ROX smFRET molecules was applied to a sample with ZMW nanoholes, and a laser beam was focused on individual ZMW nanoholes. The fluorescence of smFRET molecules was recorded using a CCD camera and a spectrometer.

To perform measurements at the single-molecule level, a certain concentration of hybrid molecules was chosen so that, at a concentration of 1.2×10^{15} cm^{-3} smFRET molecules in the buffer solution, one ZMW nanohole on average contained one smFRET molecule. Figure 3 shows an image of a single ZMW nanohole obtained with an electron microscope,

as well as a schematic arrangement of the smFRET molecule (the actual size of the hybrid molecule is several nanometers). When exciting the fluorescence of the smFRET molecule, laser radiation with a wavelength of 480 nm (the absorption line of the FAM molecule) was used, focused onto a spot with a diameter of 1 μm, which made it possible to illuminate single ZMW nanoholes, since the distance between the ZMW nanoholes on the sample was 10 μm.

Figure 3b shows the measured fluorescence spectra of the smFRET molecule in free space (black curve) and inside the ZMW (blue curve). The fluorescence spectrum of the free ROX molecule is shown in pink. As can be seen from the presented data, the fluorescence spectrum of the smFRET molecule in free space is characterized by the presence of a weak fluorescence signal in the short-wavelength part, formed by the weak fluorescence of the donor molecule of the smFRET pair, while the main share of the emission falls on the fluorescence of the acceptor molecule. This indicates a high efficiency of the FRET process, which is also in good agreement with the theory, since in the smFRET molecule the length of the linker (1 nm) is significantly less than the value of the Förster radius (6 nm). It should be noted that the fluorescence spectrum of the smFRET molecule is shifted to the red region relative to the fluorescence spectrum of the ROX molecule (the spectrum filled in pink) due to the low efficiency of excitation of high energy levels of the ROX molecule with the Förster mechanism of energy transfer (the excitation level of the acceptor molecule cannot be higher than the excitation level of the donor molecule).

When placing an smFRET molecule in a ZMW nanohole, the fluorescence spectrum shifts to the short-wave region (blue curve in Fig. 3b). In addition, the value of the wavelength of light corresponding to the fluorescence maximum has a smaller value than the corresponding value of the emission spectrum of an individual free acceptor molecule. This indicates the presence of processes of stimulated by ZMW population of the upper electron energy levels of the donor and acceptor molecules, respectively. Measurements using the example of a donor–acceptor pair show that a ZMW can strongly affect the fluorescence properties of individual quantum light emitters.

Another advantage of zero-mode waveguides is the ability to perform parallel spectral measurements with many single molecules simultaneously. In this case, the spectrum is measured from each individual molecule! This advantage of ZMW nanostructures has revolutionized single-molecule sequencing of DNA molecules in real time [64]. The main contribution to the development of these methods was made by scientific groups associated with Pacific Biosciences of California, Inc. (M Wanunu, A Wenger).

A practical solution to the problem of simultaneous (yet, independent!) spectral measurements of fluorescence of a large number of individual dye molecules (more than 1 million molecules) required the use of not only nanohole lithography methods but also new approaches to integrated optics for the simultaneous irradiation of such a huge number of ZMW nanostructures with laser radiation to excite the fluorescence of molecules in each ZMW.

To excite a dye molecule in a ZMW, it is necessary to provide laser radiation with an intensity of about 100 W cm^{-2} in the ZMW region. For a single ZMW, this is quite easy to implement by direct illumination with a laser beam focused onto a spot of small diameter. However, when using 1 million ZMWs located even at a small distance (but sufficient for resolving adjacent ZMWs in an optical microscope) from each other equal to 3 μm, the region with ZMW nanoholes will occupy an area of 9 mm^2. Therefore, to achieve an intensity of 100 W cm^{-2} in each ZMW, the laser radiation has to have a power of about 10 W, which is incompatible with the measurement conditions, since it would lead to significant heating of the reaction cell and, with a high probability, to its physical destruction.

The only possible solution to the problem of exciting a large number of ZMWs is to use planar optical waveguides placed near each ZMW in an integrated optical circuit. This method was proposed in a patent [65] and implemented in commercial Sequel sequencers manufactured by Pacific Biosciences. The arrangement of zero-mode waveguides in the exponentially decaying field emerging from the waveguide allows achieving the required intensity for excitation and registration of fluorescence of single molecules inside each ZMW of the reaction cell used. The use of integrated optical circuits has become an effective solution that allows the 'targeted' introduction of excitation radiation into the ZMW using planar waveguides. The problem of creating planar waveguides and input/output and control of radiation in such waveguides have been studied in detail previously [66]. It should be noted that the implementation of the coupling of planar waveguides with ZMW nanoholes and the manufacture of final products require the use of the most advanced techniques of modern nanooptics and nanoengineering.

Figure 4 shows a schematic diagram of the optical part of the reaction cell with 1 million ZMWs, made according to the principle described above [67]. Excitation of fluorescence inside the ZMW volume using integrated optics elements allows illuminating a huge area of the reaction cell. An array of diffraction gratings is used to couple the radiation into the optical waveguides of the reaction cell. Then, using multistage Y-shaped splitters, the radiation is divided among a large number of individual waveguides, each having thousands of ZMWs integrated into it. Each ZMW is placed near the waveguide core, and the evanescent field created by the waveguide is used to excite the fluorescence of molecules in the ZMWs. Each waveguide is a structure formed by a silicon nitride core (refractive index $n = 1.9$) and a silicon dioxide cladding (refractive index $n = 1.46$). Of major importance is the division of the optical scheme into two separate zones: the first is the excitation region, and the second is the region with ZMW nanoholes. Such a scheme allows reducing parasitic illumination from the exciting laser radiation.

3. Detection of individual biomolecules using the example of troponin molecules visualization in human blood

An example of socially significant applications, in which it is necessary to visualize and measure analyte concentrations less than 10^{10} cm^{-3}, is the detection of troponin molecules. The concentration of troponin in human blood is a marker of human cardiovascular diseases. Troponin molecules are produced in the human circulatory system during the destruction of cardiac muscle cells (cardiomyocytes) as a result of an imbalance between the demand for blood and its supply to the cardiac tissue. Troponin-C, troponin-T, and troponin-I control cardiac muscle contractions under physiological conditions. Muscle contraction develops due to the binding of Ca^{2+} ions by the troponin complex and the subsequent activation of ATP-dependent interaction of

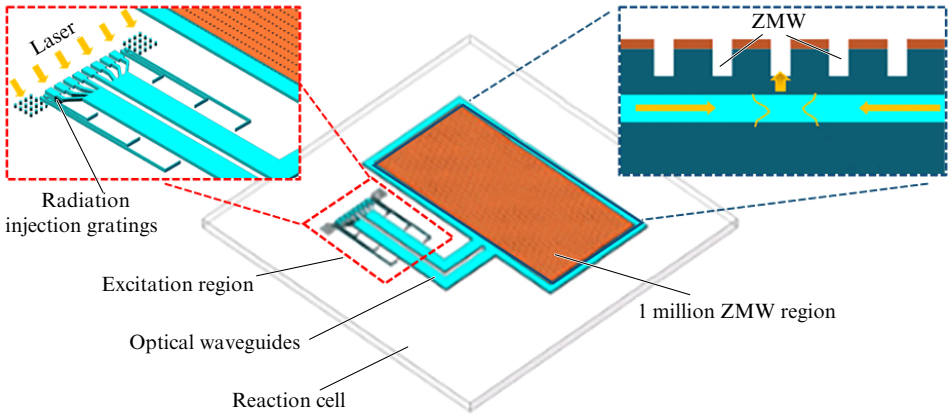

Figure 4. Schematic of reaction cell for single-molecule DNA sequencing using zero-mode waveguides (ZMW) and integrated optics methods (from Ref. [67]).

myosin with actin [68]. In the heart of healthy adults, troponins I and T are present exclusively in specific cardiac isoforms, not expressed in other tissues. Destruction of cardiac cells results in the release of these intracellular proteins into the blood plasma, which makes it possible to use cardiac tissue-specific troponin isoforms as highly specific markers of cardiomyocyte damage.

Detection of troponin molecules in human blood is considered the most direct way to detect the occurrence of serious cardiovascular diseases. It has already been clinically shown that a level of troponin in the blood of about 10^9 cm^{-3} (100 pg ml^{-1}) indicates irreversible changes in the heart muscle [21]. At the same time, the concentration of troponin molecules in the blood, reflecting the degradation of the heart muscle, increases from 10^7 cm^{-3} to 10^9 cm^{-3} (1 – 100 pg ml^{-1}) in a relatively short time, about 6 hours, which makes ultrafast measurement of troponin levels in the blood critically important for the diagnosis and treatment of cardiovascular diseases [69]. Thus, according to the recommendations of the National Academy of Clinical Biochemistry, clinical testing of blood serum samples for cardiac biomarkers should be carried out within 1 hour [70]. The threshold at which therapeutic intervention is necessary is estimated at 10^7 cm^{-3} [71].

Commercially available troponin assays have detection limits in the range of 10–80 pg ml^{-1}, detection times of 10 min–24 h, and analyte volumes of 17 µl–10 ml [21]. All of them employ preconcentration methods prior to analyte measurement. In contrast, SMCM methods allow the concentration of troponin molecules to be measured directly in human blood. The troponin-T (cTnT) molecule has enough epitopes on its surface to bind up to 30 antibodies. In the developed sample preparation protocol, a solution of antibodies against cTnT labeled with Cy 7.5 dye molecules is added to a patient's blood sample. After the antibodies bind to the troponin-T molecules, on average of about 27 such antibodies bind to one cTnT molecule. Antibodies not bound to the cTnT molecules are selectively removed from the sample. After this, the prepared sample is placed in a fluorescence microscope, which records the fluorescence of the Cy 7.5 dye molecules bound to the cTnT molecule.

Figure 5 shows images of cTnT molecules obtained by recording fluorescence in an optical chip at different concentrations in solution: (a) 1 pg ml^{-1}, (b) 100 pg ml^{-1}. The attachment of many fluorescent dye molecules to the cTnT molecule formed a bright light source observed in an optical microscope upon excitation with laser radiation. Figure 5a shows the image of a single cTnT molecule obtained at an analyte concentration of 1 pg ml^{-1} (2×10^7 cm^{-3}). The image clearly shows a bright spot corresponding to the detection of a single molecule. A CCD camera records approximately 3×10^4 photons s^{-1} from this molecule, which corresponds to the expected photon flux from a single cTnT molecule. This fact proves the recording of a single cTnT molecule. The optical image of a single cTnT molecule obtained in the presented fluorescence microscopy scheme is elongated due to aberrations of the optical microscope associated with the closure of part of the microscope objective aperture to block the exciting laser radiation. Figure 5c shows a section of a typical optical image of a single cTnT molecule dissolved in human blood serum. The figure clearly shows the parasitic luminescence of blood plasma (wide pedestal) and a narrow peak corresponding to the registration of a single cTnT molecule. As can be seen from the figure, the developed fluorescence microscopy method allows recording single biomolecules with a signal-to-noise ratio of approximately 3. In this scheme, it was possible to implement the detection of single molecules in the field of a laser beam with a diameter of 15 µm (Fig. 5a, b) due to an increase in the brightness of the detected particle. The detection volume with this registration method increases by 10^4 times relative to the method of counting single molecules in a tightly focused beam, due to which it is possible to significantly reduce the time for determining ultra-low concentrations of troponin.

The method presented allows determination of the concentration of cTnT molecules in the patient's blood

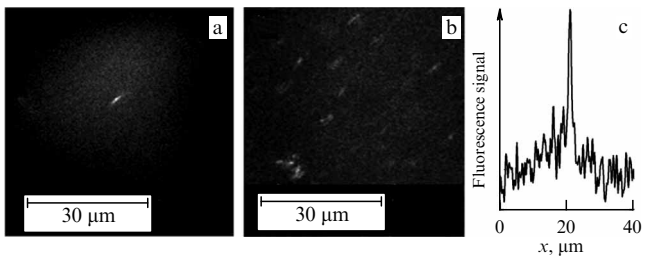

Figure 5. Optical images of troponin-T molecules at different concentrations: (a) 1 pg ml^{-1} and (b) 100 pg ml^{-1}, (c) cross-sectional image of troponin-T molecule detected in human serum sample [72].

serum with a minimum level of 1 pg ml^{-1} and an error within 40% [72], the measurement time being about 5 min, which corresponds to an order of magnitude higher sensitivity than 10–80 pg ml^{-1} in commercial test systems using sample preconcentration and 1000 times faster than any of the methods that do not use techniques to increase the concentration of analyte molecules in the sample [21]. The level of concentration determination achieved is sufficient for diagnostics of early-stage cardiovascular diseases, which was previously not possible.

4. Detection of virulent virus particles using the example of SARS-CoV-2 coronavirus visualization

Another socially significant problem that requires the use of SMCM methods is the rapid determination of the virulence of viral particles in a sample and the measurement of the ratio of viral and pseudoviral particles [73]. Recently, we were able to solve this problem for the first time using SMCM methods using the SARS-CoV-2 virus as an example [74].

The gold standard for collecting samples for SARS-CoV-2 testing is a nasopharyngeal swab. The difficulty in detecting SARS-CoV-2 directly in a swab is associated with its low concentration. The highest concentration of viral particles detected in pharyngeal swab samples reached 2.4×10^9 viral particles per 1 liter [75]. However, the number of viral copies in a swab is only $10^4 - 10^7$ viral particles per ml (10 aM–10 fM) [76]. This makes optical detection very difficult, since the average distance between virus particles in the sample volume of the swab taken is about 1 mm. Such a low concentration of virus particles requires the use of ultra-sensitive detection methods based on SMCM.

Optical diagnostics of the SARS-CoV-2 virus was implemented using fluorescent nanoparticles formed by core–shell nanostructures fabricated by introducing Cy 7.5 dye molecules into the polydopamine shell of an Au nanorod at an optimal dye concentration corresponding to the maximum suppression of polydopamine quenching [74]. Such nanoparticles are characterized by bright and stable fluorescence suitable for single virus detection, as well as (1) low photodegradation, (2) insensitivity to concentration attenuation, and (3) chemical stability and biocompatibility. Such fluorescent labels were used to label monoclonal antibodies against the SARS-CoV-2 S protein.

Figure 6a shows TEM images of two core–shell nanostructures used as fluorescent labels in SMCM microscopy of SARS-CoV-2. The TEM image clearly shows the composition of the nanostructures, including their cores and shells. The nanorods were 10 nm (diameter) $\times$ 40 nm (length), and the shell thickness was 10 nm. The shells contained about 1000 dye molecules, which corresponds to a volume concentration of about 2.5×10^{18} cm^{-3}.

Figure 6b shows the optical image of a dried nasopharyngeal swab droplet from a patient with SARS-CoV-2 coronavirus illuminated with white light. This swab containing viral particles was spiked with antibodies against the SARS-CoV-2 S-protein bound to fluorescent nanoparticles. Before the optical measurements, the concentration of virions in the sample was measured by titration. Figure 6c shows a fluorescence image (in the spectral range of 800–950 nm) of the same sample as in Fig. 6b after irradiation of the sample with laser light. This image was obtained using an epifluorescence microscopy setup by irradiating the sample with laser light with a wavelength of 780 nm and recording in a spectral window of 800–950 nm [74]. Several bright and dim spots (marked with arrows) can be seen in the image. As the measurements showed, the weak spots (marked with orange arrows) are agglomerates of the fluorescent nanoparticles used. Similar spots are also observed in control samples with fluorescent nanoparticles, but without SARS-CoV-2 virus particles. Each bright spot in Fig. 6c (marked with red arrows) corresponds to the fluorescence of nanoparticles bound via an antibody to one SARS-CoV-2 virus particle. Moreover, each bright spot contains approximately 40 fluorescent nanoparticles. Such bright fluorescent spots indicate the presence of SARS-CoV-2 virus particles in the sample.

The presence of multiple spikes on the SARS-CoV-2 viral particle allows the formation of a bright fluorescent agglomerate consisting of approximately 40 fluorescent nanoparticles. The brightness of such a nanolocalized light source is proportional to the number of spikes on its lipid membrane, which is a sign of virulence of coronavirus particles. In a separate experiment, we demonstrated the possibility of determining the virulence of coronavirus particles by counting the number of spikes using advanced SMCM microscopy. For comparative analysis, we used synthesized pseudovirus particles that contained on average only 3–10 spikes com-

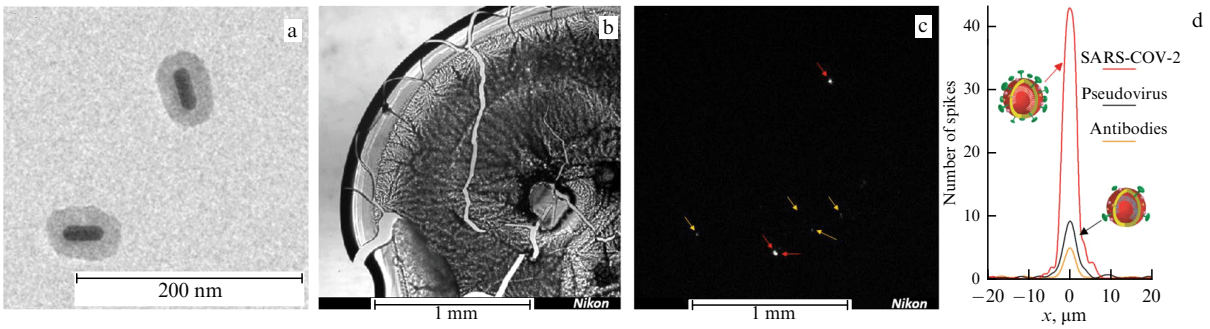

Figure 6. Detection of single SARS-CoV-2 virus particles using fluorescence measurement of core–shell fluorescent nanoparticles bound to SARS-CoV-2 antibody virions: (a) TEM image of fluorescent nanoparticles; (b) white light image of a dried droplet with core–shell nanoparticles added to it; (c) fluorescence image of the same droplet excited by 780 nm laser radiation, orange arrows indicate antibody agglomerates, red arrows indicate SARS-CoV-2 virus particles; (d) cross sections of fluorescence images of agglomerate formed by unbound antibodies labeled with core–shell nanoparticles (orange line), a pseudovirus particle (black line), and a SARS-CoV-2 virus particle (red line) [74].

pared to the 30–70 spikes on a SARS-CoV-2 virus particle. In such measurements, the amplitude of the fluorescence signal from fluorescent nanoparticles bound by antibodies in pseudovirus particles was approximately five times smaller than the corresponding signals upon detection of SARS-CoV-2 virus particles. The cross sections of the corresponding optical images are shown in Fig. 6d. As can be seen from the image, the fluorescence signal of the pseudovirus particle is significantly smaller than the signal of the SARS-CoV-2 particle and is only 50% higher in amplitude than the fluorescence signal of agglomerates formed by antibodies that have not bound to the virus particles.

The developed method of SARS-CoV-2 active virion sensing allows determining the concentration of viral particles in a sample. The demonstrated detection limit of the developed method is about 800 virions ml^{-1}. This number is limited by the rather small sample volume used, equal to 1 μl. At a concentration of 800 virions ml^{-1}, it is possible to detect only one or a few virions in such a small volume. A further increase in the sensitivity of the developed method is possible using microfluidic platforms and using larger sample volumes.

5. Visualization of toxin–receptor interaction at single-molecule level

SMCM methods implemented using zero-mode waveguides allow monitoring several single-molecule reactions simultaneously. One example is the demonstration of visualization of toxin–receptor interaction, making it possible to study the kinetics of such interaction at the single-molecule level. The method was implemented using ZMW nanostructures fabricated in aluminum. Measurements were made using a synthetic high-affinity peptide acting as a receptor and immobilized on a quartz surface, inside a ZMW nanohole, and alpha-bungarotoxin labeled with an Alexa Fluor 555 molecule. It was shown that the use of a zero-mode waveguide makes it possible: (1) to record binding at the single-molecule level for many receptor-toxin pairs simultaneously, (2) to measure the binding dynamics due to the high signal-to-noise ratio achieved in the recorded optical signal. In addition, the developed approach to sample functionalization can be used to determine low concentrations of various toxins.

Synthetic high-affinity peptide (HAP), an analogue of the nicotinic acetylcholine receptor, can be used instead of the receptor itself. It consists of 13 amino acids and has a high affinity for alpha-bungarotoxin. This toxin is one of the most frequently used tools for studying the nicotinic acetylcholine receptor and is produced in the venom glands of the snake *Bungarus multicinctus* [77]. When it is released (during a snake bite), this toxin specifically binds to the nicotinic acetylcholine receptor, blocking nephromuscular transmission.

HAP was obtained in the Department of Molecular Neuroimmune Signaling of the Institute of Bioorganic Chemistry of the Russian Academy of Sciences by solid-phase peptide synthesis. Its dimensions are 14.5 Å in height and 12 Å in diameter (cross-sectional area is ~ 1 nm^2). With the surface area of quartz in the ZMW nanohole being approximately 10^4 nm^2 , about $\sim 10^4$ HAPs can be immobilized on its surface. Toxin–receptor interaction was studied by attaching alpha-bungarotoxin labeled with the fluorophore Alexa Fluor 555 (Thermo Fisher Scientific). The degree of toxin labeling is equal to one (each toxin molecule is bound to one dye molecule).

Toxin–receptor binding was recorded using an AF555 fluorescence signal. Measurements were performed using a Nikon Eclipse Ti/U inverted microscope with an epifluorescence scheme and a Nikon 40× objective, NA = 0.6. Fluorescence was excited by laser radiation with a wavelength of 532 nm and an intensity of 200 W cm^{-2}. Registration was performed at a shifted wavelength in the spectral window of dye fluorescence (550–750 nm). Laser radiation was spectrally separated from the fluorescence signal using a dichroic mirror and an interference notch filter. The laser spot size allowed us to study the attachment reaction simultaneously in 40 zero-mode waveguides, which made it possible to collect statistics on receptor–toxin binding.

The toxin was added to the sample by applying a buffer solution with the toxin dissolved in it at a concentration of $\sim 10^{13}$ cm^{-3} to the functionalized substrate. The concentration was selected in such a way that on average there was less than one molecule of labeled toxin in one ZMW nanohole, the average number of labeled toxins in ZMW was $\sim 10^{-2}$ molecules. It is important to note that the bond between the HAP and the toxin cannot be broken without additional external influences. Therefore, if binding has occurred, the toxin molecule cannot leave the ZMW nanohole during the experiment.

Measurements at the level of single-molecule fluorescence require careful monitoring of the parasitic fluorescence of the samples used, materials of the corresponding reaction cells, and reagents. In the measurements performed, three samples were used to monitor the parasitic fluorescence level — three identical reaction cells formed by quartz substrates with 100-nm-thick aluminum films deposited on them, in which matrices with ZMW nanoholes 100 nm in diameter were created using electron lithography. Sample preparation for the first sample consisted only of using the step of passivation of the aluminum surface with poly(vinylphosphonic acid) (PVPA), necessary to prevent adsorption of biomolecules on the aluminum surface. For the second sample, a protocol of quartz surface functionalization was carried out to immobilize HAP molecules on the quartz surface inside the ZMW nanohole, but without adding HAP. For the third sample, a full functionalization protocol with HAP immobilization was carried out. During the measurements, when adding the toxin solution for the first and second samples, it is expected that the toxin will diffuse in and out of the ZMW nanohole volume in characteristic times of 10–100 μs and, thus, it will not be able to emit a significant fluorescence signal, which is effectively recorded only when the toxin molecule is in the ZMW nanohole. Only nonspecific, low-probability adhesion to the quartz bottom and walls of the well is possible. For the third sample, it is expected that the toxins will bind to the HAP and give a significant fluorescence signal.

To study the toxin–receptor interaction, the prepared reaction cells — samples with an array of ZMW nanoholes — were installed in the object plane of an optical microscope one by one. A solution of the labeled toxin was added to each cell. After a time $t = 4$ min (the characteristic time during which the receptor is bound to the toxin in ZMW), fluorescence measurements were performed in the samples. Figures 7a–c show optical images of the experimental samples obtained at the fluorescence wavelength of the AF555 dye: (a) Sample 1 after the step of applying polyvinylphosphonic acid, PVPA; (b) Sample 2 after the click chemistry reaction; (c) Sample 3 after the complete functionalization protocol with attached HAP. Bright dots

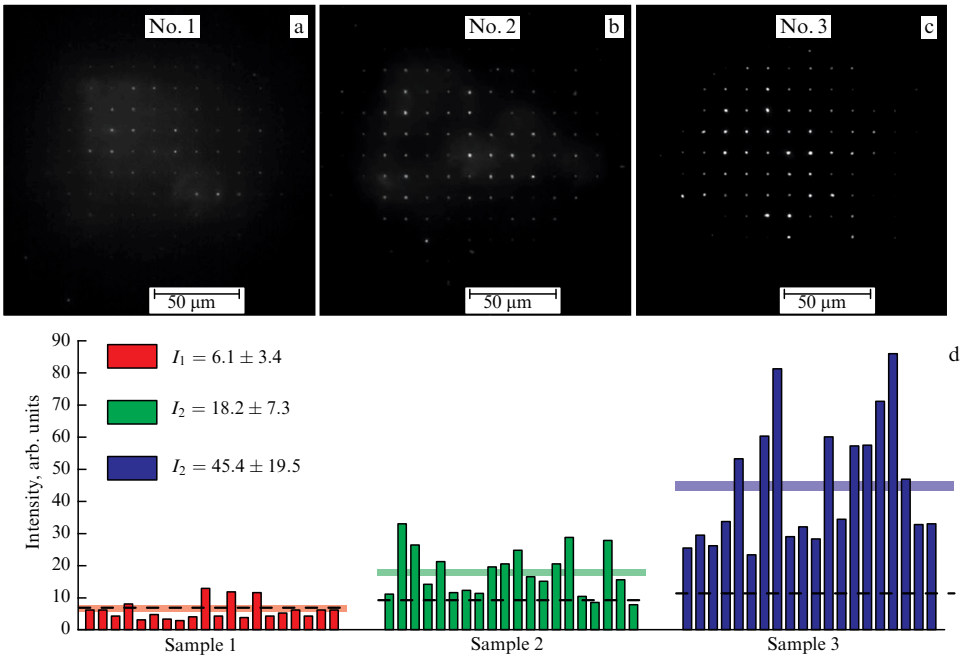

Figure 7. Image of ZMW nanohole array obtained at fluorescence wavelength of AF555 dye molecules for three samples during receptor–toxin binding observation: (a) Sample 1 after the step of PVPC deposition; (b) Sample 2 after click chemistry reaction; (c) Sample 3 after full functionalization protocol with attached HAPs; (d) histogram showing fluorescence signal level for all three samples; horizontal semi-transparent lines show average fluorescence signals, black dashed lines are parasitic fluorescence level before addition of toxin.

correspond to the fluorescence signal recorded in the ZMW nanoholes. This signal is formed by parasitic fluorescence for Samples 1 and 2, and only for Sample 3 are both parasitic fluorescence and fluorescence of toxins labeled with the AF555 molecule and bound to the HAP at the bottom of the ZMW nanoholes formed.

In Figure 7d, the histograms of different colors show the fluorescence intensities of 20 individual ZMW nanoholes for different samples: the fluorescence intensities of ZMW nanoholes on Sample 1 are marked in red, on Sample 2, in green, and on Sample 3, in blue. The average fluorescence signals are shown as semitransparent horizontal lines: for Sample 1, the average signal was 6.1 ± 3.4, for Sample 2, it was 18.2 ± 7.3, and for Sample 3, it was 45.4 ± 19.5. It is important to note that, for Sample 1 (passivation of aluminum with PVPA), the average fluorescence signal (6.1 ± 3.4) did not change within the error bar compared to the parasitic fluorescence level (7.5 ± 2.6) after adding the labeled toxin. The reason is the low concentration of labeled toxins in the solution. Thus, on average, there is one labeled toxin for every 100 ZMW nanoholes and there is no specific binding. For Sample 2 (the sample after the click chemistry step, but without HAP), the average fluorescence signal increased approximately twofold compared to the parasitic fluorescence, from 9.4 ± 3.0 to 18.2 ± 7.3. This is explained by the fact that, because of the functionalization of the sample, a complex of organic molecules for the immobilization of HAP was formed at the bottom of the ZMW, where the toxin molecules can be localized. For Sample 3 (the sample with immobilized HAP), the average signal upon addition of the toxin increased more than fourfold, from 10.9 ± 5.5 to 45.4 ± 19.5, which reflects the specific binding of HAP to the toxin.

Figure 8a shows an image of the ZMW nanohole array obtained at the fluorescence wavelength of AF555 dye molecules. Three ZMW nanoholes for which the time dependence of the fluorescence signal was measured are marked with colored circles. Figures 8b–d show the time dependences of the fluorescence signal for the ZMW nanoholes marked with colored circles in Fig. 8a. The plots show a stepwise increase in the signal with approximately the same difference in the signal amplitude for each such 'step,' which is characteristic of the dynamics observed when registering events with single-molecule accuracy. This form of the signal is associated with single events of attaching the labeled toxin to the immobilized HAP. The amplitude of the signal increase for each attachment event is slightly different but remains comparable. The differences may be related to the orientation of the dye molecules relative to the excitation field, as well as to the attachment of the toxin to the HAPs located at different points of the ZMW nanohole — the excitation field is highly non-uniform inside the ZMW nanohole (Fig. 2c), which affects the recorded photon flux.

The results obtained show that the use of zero-mode waveguides in combination with SMCM techniques allows recording the toxin–receptor interaction at the level of single molecules. For the first time, the fundamental possibility of observing the single-molecule dynamics of the interaction of receptor and toxin molecules has been demonstrated.

6. Single-molecule DNA sequencing

The development of single-molecule sequencing methods is a relevant and rather complex scientific problem of high practical and social significance. Projects aimed at creating sequencers that allow full-genome sequencing are among the central projects at the state level in various countries [78]. Breakthrough technologies of massively parallel sequencing (MPS) of DNA, which have ensured rapid progress in recent years, have shown significant limitations: (1) the impossibility of accurately decoding extended sections of DNA, (2) the

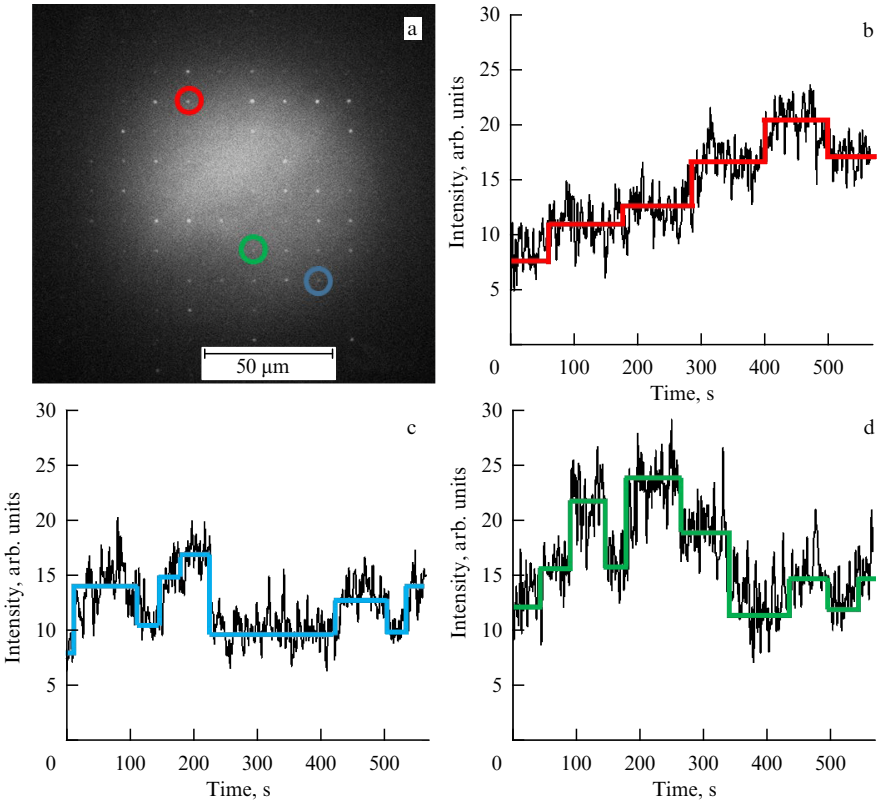

Figure 8. Measured single-molecule dynamics of receptor–toxin binding: (a) image of ZMW nanohole array obtained at fluorescence wavelength of AF555 dye molecules, observing receptor–toxin binding at single level (three ZMW nanoholes, for which time dependence of fluorescence signal is shown, are marked with colored circles); (b) time dynamics for ZMW nanohole marked with a red circle; (c) time dynamics for ZMW nanohole marked with a blue circle; (d) time dynamics for ZMW nanohole marked with a green circle.

process of preparing material for research requires its amplification, which is associated with the generation of errors, as well as with partial loss of important information, (3) the high cost of devices and associated reagents significantly limit their use.

The exponential growth in DNA sequencing productivity observed between 2008 and 2013 stopped after 2016, when the cost of decoding one human genome was fixed at around $1,000. The drop in cost was due to significant progress in massively parallel DNA sequencing technologies, which have actually reached their limit in both productivity and cost. The bottleneck in increasing the scale and range of population studies is currently the cost of sequencing, which, for the technologies of massively parallel DNA sequencing dominant in the genomic research market today, is more than 30,000 rubles per billion nucleotides (1 Gb). A further reduction in the cost is possible only by increasing the productivity of DNA sequencing.

The rapid development of second-generation sequencing technologies has provided enormous opportunities for scientific molecular genetic research and opened a huge market for related services. At the same time, new opportunities have generated new demands. The problems that are difficult or impossible to solve using short DNA reads are becoming increasingly clear. Thus, the study of complex microbial communities using a fragment of a 16S rRNA gene with short reads has limited resolution, and metagenomic studies based on whole-genome sequencing are expensive and complex. Meanwhile, metagenomic studies are used in fundamental biology, as well as in medicine, biotechnology, agriculture, the food industry, forensics, and even matters of preserving cultural heritage [79, 80]. Considering the One Health program announced by the WHO, the study of viromes (viral components of microbiomes) in domestic and farm animals is of particular importance [81].

The development of new single-molecule sequencing methods is relevant for both worldwide science in general and Russian science in particular. Sequencing single DNA molecules is a complex scientific and technical problem that has remained relevant for more than 20 years. The solution to this problem itself will bring to a new level the capabilities of molecular genetics, which is increasingly in demand both in fundamental biology and in medicine, forensics, the food industry, and other areas of human activity. We should also note the gigantic social aspect associated with the development of personalized medicine and new methods of diagnosis and treatment of a number of serious human diseases (oncological diseases, diseases of the immune and nervous systems), the development of approaches to significantly extend the duration of active human life, etc.

Single-molecule sequencing methods solve the problem of determining the species composition of microbial communities by reading the entire ribosomal operon, which allows a more accurate identification of microorganisms. Greater accuracy can also be achieved with metagenomic whole genome sequencing (mWGS) [82]. During coronavirus outbreaks and regular seasonal outbreaks of viral respiratory diseases, the task of rapid sequencing viruses and viral quasispecies is becoming relevant for epidemiology. Using nanopore sequencing and single molecule real time (SMRT)

sequencing as examples, the possibility of sequencing entire viral genomes has been demonstrated, which allows distinguishing viral haplotypes within the virome [83].

It is worth noting the complex interdisciplinary nature of the single-molecule sequencing problem. The range of problems to be solved relates to different fields of science: genomics, biophysics, biochemistry, physics, optics, materials science, etc., as well as the problem of identifying a specific nucleotide sequence. In developing single-molecule sequencing methods, it is necessary to solve a number of important problems aimed at improving reagent synthesis methods, ultrafast detection of labeled nucleotide fluorescence, and spatial manipulation (with nanometer resolution) of single polymerase molecules and DNA molecules associated with them. This will also significantly expand scientific knowledge and control methods (chemical, optical, physical) at the level of individual biomolecules, which, in turn, will make it possible to solve a number of important problems in the field of sensorics, highly sensitive diagnostics, and visualizing biological objects; to obtain new knowledge in the fields of biochemical and biophysical processes, and genomics at the level of individual biomolecules; and also to develop new control methods (physical, chemical, optical) of individual biomolecules at the nanoscale.

Third-generation sequencers available on the world market today cannot satisfy the entire demand for these technologies. The greatest difficulty arises with consumables, which have a fairly high cost due to the complexity of their production and compatibility with the single-molecule sensitivity level, which imposes significant restrictions on the purity and efficiency of the corresponding reagents and reaction cells for sequencing. In addition, they may be unavailable for work due to the remoteness of sequencing centers or even for political reasons: existing foreign third-generation sequencing technologies are dual-use technologies and therefore access is limited; sequencing data is processed on foreign servers, access to which may be limited; the sale of sequencing reagents may be subject to sanction restrictions for deliveries to a number of countries; the creation of reaction cells for sequencing requires access to modern optical nanolithography technologies (at the time of writing this review, there are no such production facilities in the Russian Federation).

In the Russian Federation, the development of an optical single-molecule DNA sequencer was organized by the Institute for Analytical Instrumentation, RAS and carried out jointly with Syntol LLC (development and manufacturing of sequencing reagents), Institute of Spectroscopy, RAS (development and manufacturing of the optical detector), as well as the Bauman Moscow State Technical University (development and manufacturing of reaction cells). Figure 9b shows an optical diagram of the sequencer, implemented in the corresponding prototype of the single-molecule sequencing hardware and instrument complex (APCOS) (Fig. 9c).

In the created sequencer, the nucleotide sequence of a DNA molecule is determined during its replication by an enzyme, the phi29 polymerase immobilized inside a ZMW nanohole on the quartz surface (the so-called bottom of the nanowell formed by the ZMW nanohole). The polymerase completes the DNA molecule being sequenced using labeled (with fluorescent dye molecules; see below) hexaphosphates added in abundance to the buffer solution. The nucleotide embedded from the hexaphosphate is complementary to the nucleotide in the DNA chain being sequenced, located in the polymerase activity zone. In this case, the fluorescent dye molecule is released. For a certain type of nucleotide embedded by the polymerase, it is essential that the hexaphosphates in the buffer solution have individual labels. For example, the hexaphosphate with the A-nucleotide is labeled with the molecule Cy 3, the hexaphosphate with the T-nucleotide, with the molecule Cy 3.5, the hexaphosphate with the G-nucleotide, with the molecule Cy 5, and the hexaphosphate with the C-nucleotide, with the molecule Cy 5.5. Each type of the given dye molecules has a distinctive characteristic fluorescence spectrum. The idea of single-molecule optical sequencing reduces to the implementation of error-free functioning of the enzyme and the determination of the fluorescence spectrum of the hexaphosphate label, the nucleotide of which is built into the DNA chain complementary to the decoded one.

In order to perform DNA sequencing and obtain information about the nucleotide sequence, it is necessary to ensure that the following operations are carried out: (1) passivation of the surface of the reaction cell with ZMW nanoholes with polyvinylphosphonic acid to suppress the adhesion of the molecules used in the sequencing reaction to the surface of the aluminum film [84]; (2) functionalization of the quartz surface located inside the ZMW nanohole — at this stage, a chemical reaction is carried out, as a result of which a complex of biotin–streptavidin molecules is covalently bound to the quartz surface, and phi29 polymerase subsequently binds to it; (3) preparation of the reaction mixture with the DNA molecule to be sequenced to create a ring-shaped DNA complex containing a DNA molecule, a primer (necessary for binding DNA to the polymerase), biotinylated phi29 DNA polymerase, and adapters used to create the ring-shaped molecule (Fig. 10); (4) performing a reaction of binding the DNA complex created in the previous step with a magnetic microbeads; (5) installing the reaction cell in the sequencer; (6) loading the DNA complex into the reaction cell with an array of ZMW nanoholes using a permanent magnet; at this step, the DNA complex is immobilized inside the ZMW nanohole by means of a biotin–streptavidin bond, which is significantly stronger than the bond used between the DNA complex and the magnetic microparticle (loading is performed by long-term movements (up to 20 min) of the magnetic beads with the complexes along the surface of the

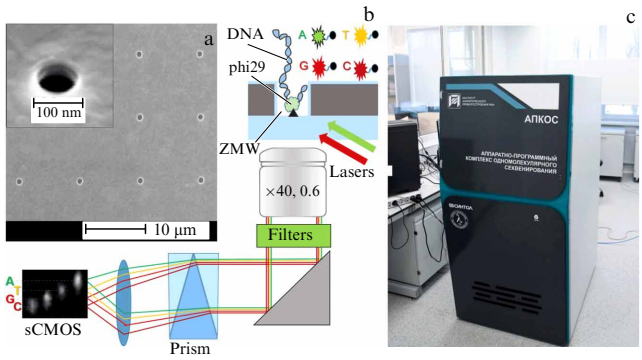

Figure 9. Single-molecule DNA sequencer (APCOS). (a) Image of ZMW array. (b) Simplified diagram of APCOS optical detector, placement of a DNA molecule with phi29 polymerase in ZMW and labeled hexaphosphates (A, T, G, C), and an image from sCMOS (scientific Complementary Metal–Oxide–Semiconductor) camera used to record weak optical signals. (c) Photograph of a pilot sample of APCOS single-molecule DNA sequencing device.

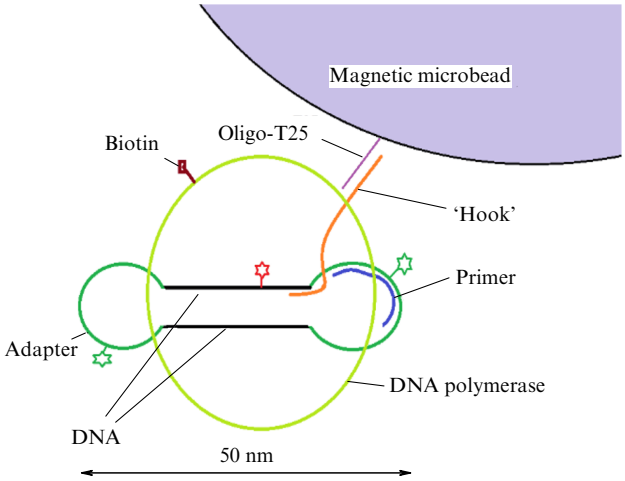

Figure 10. Structure of loaded DNA complex. Figure schematically shows composition of complex loaded into ZMW nanohole using magnetic microbeads.

reaction cell — the movements are achieved by using the forces of magnetic attraction to the magnet, which periodically changes position); (7) introducing fluorescently labeled hexaphosphates in a buffer solution into the reaction mixture; (8) turning on laser radiation sources with wavelengths of 532 nm and 640 nm; (9) registration by fluorescence of events of nucleotide incorporation into a DNA complex in an array of ZMW nanoholes; (10) identification of fluorescence spectra of dye molecules associated with the incorporated nucleotide; (11) formation and analysis of the sequence of incorporated nucleotides.

Figure 10 schematically shows the composition of the DNA complex loaded into the zero-mode waveguide using magnetic microbeads. The basis of the complex is circular DNA from 266 to 20,000 nucleotides in length, phi29 polymerase on adapters (synthesized nucleotide sequences for linking two complementary chains of a part of the DNA molecule), which contain R6G and ROX dye labels to control the efficiency of loading into the ZMW.

The created DNA sequencer implements spectroscopy of single fluorescent molecules. Spectrum measurement is performed using a prism spectrometer, which simultaneously forms a fluorescent image of a cell with ZMW nanoholes and fluorescence spectra of single molecules located in the ZMW nanoholes. This is the so-called imaging spectrometer. Simultaneous acquisition of an optical image and a fluorescence spectrum becomes possible when using a prism with a small dispersion (see Fig. 9), which allows obtaining an image of a matrix of ZMW nanoholes with a small shift along one of the coordinates on the monitor screen. This shift, on the one hand, depends on the wavelength of the radiation (due to the spectral dispersion of the prism used); on the other hand, it is not very large in amplitude, so that there is no overlapping of the images of adjacent ZMW nanoholes.

Figure 11 shows the spectral separation of four fluorescence channels in the optical detector of the sequencer, demonstrating the principle and possibility of identifying the type of labeled nucleotide by the fluorescence spectrum of a single molecule in a ZMW nanohole. The figure shows images obtained by passing light through the ZMW nanoholes in the reaction cell. They are formed using light with different wavelengths: Fig. 11a corresponds to the fluorescence of labeled nucleotide A (bound to the Cy 3 molecule), Fig. 11b corresponds to the fluorescence of labeled nucleotide T (bound to the Cy 3.5 molecule), Fig. 11c corresponds to the fluorescence of labeled nucleotide G (bound to the Cy 5 molecule), and Fig. 11d corresponds to the fluorescence of labeled nucleotide C (bound to the Cy 5.5 molecule). The horizontal lines show the expected location of the zero-mode waveguide image for each nucleotide type.

Figure 12 shows the results of the created sequencer, demonstrating the formation of a nucleotide sequence based on detector signals from all four of its registration channels during single-molecule sequencing. The results of measuring the nucleotide sequence of the synthesized oligonucleotide using phi29 DNA polymerase for 100 s using 532-nm and 640-nm laser excitation in a ZMW nanohole are shown. The dashed line shows the level above which nucleotide incorporation events are registered by the polymerase. The upper part of the figure shows a certain nucleotide sequence.

7. Conclusion

The current level of development of single molecule fluorescence registration methods, with the simultaneous use of nanophotonics, nanolithography, and integrated optics technologies, has brought together many important tools for sensorics, biology, virology, and genetics. The examples presented in this review are only a small part of the results obtained in the field of application of single molecule registration and counting methods when registering the fluorescence of dye molecules and fluorescent nanoobjects.

Worth noting is the significant progress in other areas of single-molecule detection based on recording pH values and electrophoretic currents, which are used not only in scientific research but also in commercial devices [78].

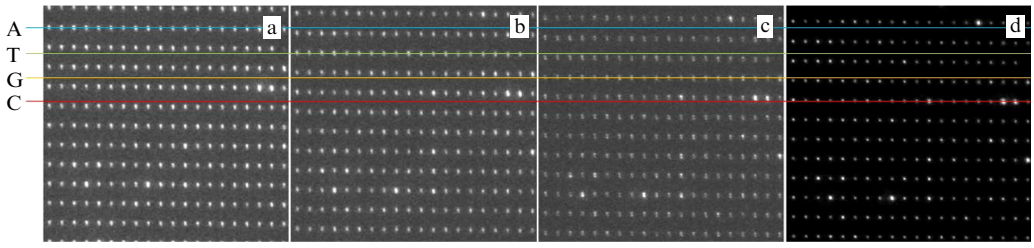

Figure 11. Spectral separation of four fluorescence channels in optical detector of sequencer. Images obtained by passing light of different wavelengths through ZMW nanoholes in reaction cell are shown. They were formed using light of (a) fluorescence of labeled nucleotide A, (b) fluorescence of labeled nucleotide T, (c) fluorescence of labeled nucleotide G, (d) fluorescence of labeled nucleotide C. Horizontal lines show expected location of zero-mode waveguides for each type of nucleotide.

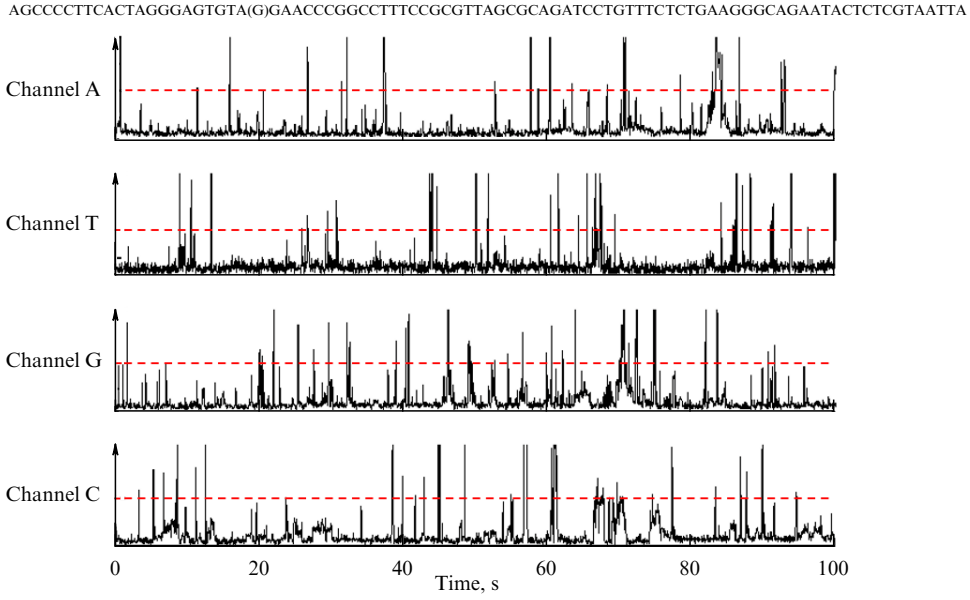

Figure 12. Recorded time-dependent signals of single-molecule sequencing. Results of measurements of nucleotide sequence of a model synthetic template (artificially synthesized DNA molecule with a known nucleotide sequence) using DNA polymerase phi29 are shown for 100 s when using 532-nm and 640-nm laser excitation in a ZMW nanohole. Dashed line shows level above which nucleotide incorporation events by the polymerase are detected. Upper part of figure shows nucleotide sequence determined by the optical detector.

Using the capabilities of modern nanolithography allows significant scaling of the number of simultaneously performed single-molecule measurements. Thus, modern platforms are already capable of monitoring single-molecule reactions with 25 million single molecules simultaneously [85]. Methods for processing the corresponding images using artificial intelligence are actively developing, which makes it possible to significantly increase the spatial density of optical images [86, 87].

Acknowledgments

The research was carried out within the framework of the FFUU-2024-003 project of the Institute of Spectroscopy of the Russian Academy of Sciences. Part of the research was carried out with the financial support from the Russian Science Foundation, project no. 23-42-00049. The work on the creation of a single-molecule optical sequencer was carried out within the framework of the research program of the Ministry of Science and Higher Education of the Russian Federation (project no. 075-15-2021-1057, lead organization — Institute for Analytical Instrumentation of the Russian Academy of Sciences).

References

1. Nayak K P et al. *Opt. Express* **15** 5431 (2007)
2. Akimov A V et al. *Nature* **450** 402 (2007)
3. Xie X S, Dunn R C *Science* **265** 361 (1994)
4. Rossier J F *Nature Mater.* **12** 480 (2013)
5. Wallquist M et al. *Phys. Scr.* **2009** (T137) 014001 (2009)
6. Koch J et al. *Phys. Rev. B* **70** 195107 (2004)
7. Hugel T et al. *Science* **296** 1103 (2002)
8. Ritter J G et al. *PLoS ONE* **5** (7) e11639 (2010) https://doi.org/10.1371/journal.pone.0011639
9. Liu Z, Lavis L D, Betzig E *Mol. Cell* **58** 644 (2015)
10. Yanagida T, Ishii Y (Eds) *Single Molecule Dynamics in Life Science* (Weinheim: Wiley-VCH Verlag, 2008)
11. Levi V, Gratton E *Cell Biochem. Biophys.* **48** 1 (2007)
12. Goodhill G J *Trends Neurosci.* **39** (4) 202 (2016)
13. Zlatanova J, van Holde K *Mol. Cell* **24** 317 (2006)
14. Miller H et al. *Rep. Prog. Phys.* **81** 024601 (2018)
15. Lu H P, Xun L, Xie X S *Science* **282** 1877 (1998)
16. Liang W et al. *Nature* **417** 725 (2002)
17. Todd J et al. *Clin. Chem.* **53** 1990 (2007)
18. Ma F et al. *Acc. Chem. Res.* **49** 1722 (2016)
19. Taylor A B, Zijlstra P *ACS Sensors* **2** 1103 (2017)
20. Walt D R *Anal. Chem.* **85** 1258 (2013)
21. Upasham S, Tanak A, Prasad S *Adv. Health Care Technol.* **4** 1 (2018)
22. Moerner W E *J. Phys. Chem. B* **106** 910 (2002)
23. Balykin V I et al. *JETP Lett.* **26** 357 (1977); *Pis'ma Zh. Eksp. Teor. Fiz.* **26** 492 (1977)
24. Personov R I et al. *Sov. Phys. JETP* **38** 912 (1974); *Zh. Eksp. Teor. Fiz.* **65** 1825 (1973)
25. Naumov A V, Vainer Yu G *Phys. Usp.* **52** 298 (2009); *Usp. Fiz. Nauk* **179** 322 (2009)
26. Eremchev I Yu et al. *Phys. Usp.* **65** 617 (2022); *Usp. Fiz. Nauk* **192** 663 (2022)
27. Novotny L, Hecht B *Principles of Nano-Optics* (Cambridge: Cambridge Univ. Press, 2012)
28. Chen D, Dovichi N J *Anal. Chem.* **68** 690 (1996)
29. Matthews J C *Fundamentals of Receptor, Enzyme, and Transport Kinetics* (Boca Raton, FL: CRC Press, 1993)
30. Karlsson R *Anal. Biochem.* **221** (1) 142 (1994)
31. Latour R A *J. Biomed. Mater. Res. A* **103** 949 (2015)
32. Zijlstra P, Paulo P M R, Orrit M *Nature Nanotechnol.* **7** 379 (2012)
33. Weiss S *Science* **283** 1676 (1999)
34. Yang Y et al. *Chem. Rev.* **113** 192 (2013)
35. Sun W et al. *Chem. Rev.* **116** 7768 (2016)
36. Baldo M A, Thompson M E, Forrest S R *Nature* **403** 750 (2000)
37. Michalet X et al. *Science* **307** 538 (2005)
38. Min Y et al. *Nanomaterials* **4** 129 (2014)
39. Chudakov D M et al. *Physiol. Rev.* **90** 1103 (2010)
40. Demtröder W *Laser Spectroscopy 1*: *Basic Principles* 5th ed. (Berlin: Springer, 2014)
41. Wang J-H et al. *Laser Photon. Rev.* **16** 2100622 (2022)
42. Doronin I V et al. *Nanoscale* **16** 14899 (2024)
43. Gritchenko A S et al. *Nanoscale* **14** 9910 (2022)
44. Lebedev D V et al. *Adv. Opt. Mater.* **12** 2400581 (2024)
45. Beliaev L Yu, Takayama O, Melentiev P N, Lavrinenko A V *Opto-Electron. Adv.* **4** 210031 (2021)

46. Hirschfeld T *Appl. Opt.* **15** 2965 (1976)
47. Widengren J, Rigler R *Bioimaging* **4** (3) 149 (1996)
48. Munkhbat B et al. *Sci. Adv.* **4** eaas9552 (2018)
49. Doronin I V et al. *Nano Lett.* **22** 105 (2022)
50. Balykin V I, Melentiev P N *Phys. Usp.* **61** 133 (2018); *Usp. Fiz. Nauk* **188** 143 (2018)
51. Maier S A *Plasmonics*: *Fundamentals and Applications* (New York: Springer, 2007)
52. Melentiev P N, Balykin V I *Phys. Usp.* **62** 267 (2019); *Usp. Fiz. Nauk* **189** 282 (2019)
53. Klimov V *Nanoplasmonics* (New York: Jenny Stanford Publ., 2014) https://doi.org/10.1201/b15442
54. Levene M J et al. *Science* **299** 682 (2003)
55. Bethe H A *Phys. Rev.* **66** 163 (1944)
56. Crouch G M, Han D, Bohn P W *J. Phys. D* **51** 193001 (2018)
57. Rigneault H et al. *Phys. Rev. Lett.* **95** 117401 (2005)
58. Entzeroth M, Flotow H, Condron P *Curr. Protocols Pharmacol.* **44** 9.4 (2009) https://doi.org/10.1002/0471141755.ph0904s44
59. Miyake T et al. *Anal. Chem.* **80** 6018 (2008)
60. Chen J et al. *Proc. Natl. Acad. Sci. USA* **111** 664 (2013)
61. Baek S et al. *Anal. Chem.* **94** 3970 (2022) https://doi.org/10.1021/acs.analchem.1c05091
62. Punj D et al. *WIREs Nanomed. Nanobiotechnol.* **6** 268 (2014) https://doi.org/10.1002/wnan.1261
63. Jackson J D *Classical Electrodynamics* 3rd ed. (New York: Wiley, 1999)
64. Eid J et al. *Science* **323** 133 (2009)
65. Zhong C F et al. "Substrates and optical systems and methods of use thereof," CA2737505C (2009); https://patents.google.com/patent/CA2737505C/
66. Kogelnik H *IEEE Trans. Microwave Theory Tech.* **23** (1) 2 (1975); Translated into Russian: *Usp. Fiz. Nauk* **121** 695 (1977)
67. Pengfei Y et al. *Opt. Precision Eng.* **30** (1) 62 (2022)
68. Katrukha I A *Biochemistry Moscow* **78** 1447 (2013) https://doi.org/10.1134/S0006297913130063
69. Hamm C W et al. *Eur. Heart J.* **32** 2999 (2011)
70. Shah A S V et al. *Lancet* **386** 2481 (2015)
71. Babuin L, Jaffe A S *CMAJ* **173** 1191 (2005)
72. Melentiev P N et al. *ACS Sens.* **5** 3576 (2020)
73. Bhat T, Cao A, Yin J *Viruses* **14** 383 (2022)
74. Kudryavtsev D S et al. *Nanoscale* **16** 12424 (2024)
75. Wölfel R et al. *Nature* **581** 465 (2020)
76. Wang W et al. *JAMA* **323** 1843 (2020) https://doi.org/10.1001/jama.2020.3786
77. Tsetlin V I *Trends Pharmacol. Sci.* **36** 109 (2015)
78. Shendure J et al. *Nature* **550** 345 (2017)
79. Shendure J, Ji H *Nat. Biotechnol.* **26** 1135 (2008)
80. Frankish A et al. *Nucl. Acids Res.* **47** D766 (2019)
81. Djordjevic S P et al. *Nat. Rev. Genet.* **25** 142 (2024)
82. Thomas T, Gilbert J, Meyer F *Microbial Inform. Exp.* **2** 3 (2012) https://doi.org/10.1186/2042-5783-2-3
83. Rubio L, Galipienso L, Ferriol I *Front. Plant Sci.* **11** 1092 (2020) https://doi.org/10.3389/fpls.2020.01092
84. Korlach J et al. *Proc. Natl. Acad. Sci. USA* **105** 1176 (2008)
85. "25 million ZMW SMRT Cell." PacBio, https://www.pacb.com/revio/
86. Dias R, Torkamani A *Genome Med.* **11** 70 (2019)
87. Novakovsky G et al. *Nat. Rev. Genet.* **24** 125 (2023)